Electronic Supplementary Information (ESI)

$A_3Mn_2Sb_3S_8$ (A = K, Rb): A new type of multifunctional infrared nonlinear optical materials based on unique three-dimensional open frameworks

Yu Xiao,‡[a] Man-Man Chen,‡[b,c,d] Ya-Ying Shen,[a] Peng-Fei Liu,[e] Hua Lin,*[b,d] and Yi Liu*[,a]

[a]*Institute for Composites Science Innovation (InCSI), School of Materials Science and Engineering, Zhejiang University, Hangzhou 310027, China*

[b]*Fujian Science & Technology Innovation Laboratory for Optoelectronic Information of China, Fuzhou, Fujian 350108, China*

[c]*State Key Laboratory of Structural Chemistry, Fujian Institute of Research on the Structure of Matter, Chinese Academy of Sciences, Fuzhou 350002, China*

[d]*University of Chinese Academy of Sciences, Beijing 100049, China*

[e]*Spallation Neutron Source Science Center, Institute of High Energy Physics, Chinese Academy of Sciences, Dongguan 523803, China*

‡*Y. Xiao and M. M. Chen contributed equally to this work.*

*E-mail: liuyimse@zju.edu.cn and linhua@fjirsm.ac.cn.

Electronic Supplementary Information Index

1. Experimental Section

1.1 Materials and Instruments

All reagents used in the present experiments were purchased from commercial sources and directly used without further purification. The optical diffuse reflectance spectra were performed on a Perkin-Elmer Lambda 900 UV–vis-NIR spectrometer equipped with an integrating sphere at room temperature. $BaSO_4$ was used as 100 % reflectance reference, and the polycrystalline samples were prepared by grinding single crystals into fine powder before the measurements. The absorption (α/S) data were converted from diffuse reflectance spectra using the Kubelka–Munk function: $\alpha/S = (1-R)^2/2R$, in which R is the reflectance at a given wavelength, α is the absorption coefficient, and S is the scattering coefficient.[1] The elemental analyses were examined with the aid of an EDX-equipped JEOL/JSM-6360A SEM. Powder X-ray diffraction (PXRD) analysis was carried out in a Rigaku Mini-Flex 600 powder diffractometer (Cu-K_α, λ = 1.5418 Å). The direct current magnetic susceptibility was measured using a Quantum Design PPMS-9 T magnetometer at a field of 5000 Oe in the temperature range of 2–300 K. The handpicked single crystals were ground to fine powder to minimize possible anisotropic effects and loaded into a gelatin capsule. The data were corrected for the susceptibility of the container and for the diamagnetic contribution from the ion core. The photo-electrochemical tests were done under simulated solar light illumination using an electrochemical workstation (CHI660E) with conventional three-electrode setup. Each as-prepared powder sample was coated onto a slice of ITO glass with an area of 0.5×1 cm^2 and employed as the working electrode. A saturated

Hg/Hg_2Cl_2 and a platinum wire were used as the reference and counter electrodes, respectively, and 0.2 M Na_2SO_4 aqueous solution was used as electrolyte. A 500 W Xe lamp was utilized as the simulated solar light source.

1.2 Synthesis

All chemical reagents used in the present experiments were commercially available, no further purification were performed. Ammonia solution (AR, 25–28%), hydrazine monohydrate (98%) and PEG-400 (>99.5%) were purchased from Sinopharm Chemical Reagent Co., Ltd. Mn powder (>99.95%), K_2CO_3 (AR, >99%), Rb_2CO_3 (AR, >99%), S powder (AR, >99.5%) and Sb_2S_3 (>99.9%) were purchased from Aladdin Co., Ltd.

Dark-red crystals of $K_3Mn_2Sb_3S_8$ were synthesized by the following reactions: 1.0 mmol of K_2CO_3, 2.0 mmol of Mn, 0.5 mmol of Sb_2S_3, 2.0 mmol of S, 1.5 mL of hydrazine monohydrate (98%) and 2.0 mL PEG-400 were mixed together and sealed in a 25 mL Teflon-lined stainless autoclave and heated at 413 K for 7 days. The resultant reaction mixtures were washed with deionized water and ethanol, respectively, and the yield is about 70% (based on Mn). When Rb_2CO_3 was used instead of K_2CO_3, dark-red crystals of $Rb_3Mn_2Sb_3S_8$ can be obtained through the same method, and the yield is approximately 85% (based on Mn).

1.3 Second-Harmonic Generation (SHG) Measurements

The powder SHG measurements were carried out with the Kurtz-Perry method using a 2050 nm Q-switch laser.[2] $AgGaS_2$ was used as a benchmark material, which is provided by Anhui Institute of Optics and Fine Mechanics, Chinese Academy of

Sciences. $A_3Mn_2Sb_3S_8$ (A = K, Rb) and $AgGaS_2$ were ground and sieved into distinct particle size ranges (30−46, 46−74, 74−106, 106−150, 150−210 μm). The SHG signals of the frequency-doubled output emitted from the sieved samples were detected using a photomultiplier tube and recorded on the oscilloscope.

1.4 Laser Induced Damage Threshold (LIDT) Measurements

The LIDTs of $A_3Mn_2Sb_3S_8$ (A = K, Rb) at the range of 150−210 μm were measured through single pulse measurement method[3] and crushed $AgGaS_2$ single crystal as the reference. Both samples were packed into identical plastic holders (thickness: 1 mm and diameter: 8 mm). After being exposed to the high-power 1064 nm laser radiation with pulse width τ_p of 10 ns, the apparent change of sample was monitored by an optical microscope. The power of laser beam and the damage spot radius were respectively measured by a Nova II sensor with a PE50-DIF-C energy sensor and a Vernier caliper.

1.5 Single-Crystal Structure Characterizations

Room-temperature single-crystal XRD data were collected on an Oxford Xcalibur (Atlas Gemini ultra) diffractometer with a graphite-monochromated Mo-K_α radiation (λ = 0.71073 Å). The absorption correction was done by the multi-scan method.[4] The direct methods was adopted to solve the crystal structure, and refined by the full-matrix least-square fitting on F^2 using the *SHELX–2014* program package.[5] Take $K_3Mn_2Sb_3S_8$ as an example, the assignments of K, Mn, Sb, and S were determined on the basis of the interatomic distances and relative displacement parameters. All of the atoms were refined with anisotropic thermal parameters and a secondary extinction

correction. The final atomic positions were standardized with the *Structure Tidy* program.[6] The structure was solved and refined successfully in the $I\bar{4}2m$ (No.121) space group. After the first refinement, the isotropic temperature factors for three K atoms and large R values of R_1 = 0.0974 and wR_2 = 0.2109. In the following refinement, the occupancies of three K atoms were allowed to free refinement, and the occupancies of 100, 91.06 and 9.02% for K1, K2 and K3, respectively, were obtained. To satisfy the charge balance requirements, the sum of the occupancy of K2 and K3 was constrained to be 1.0; after this procedure, the occupancies of K2 and K3 were 91.1 and 8.9%, respectively. Note that the S5 atom was refined as split site (e.g., S5A, and S5B) due to the high atomic displacement parameter and the occupancies were refined to 50%, and 50%, respectively. Crystallographic information and selected bond distances for the title compound are summarized in Tables 1–3. CCDC number: 2060369–2060370.

2. Computational Details

The DFT calculations have been performed using the *Vienna ab initio simulation package* (VASP)[7–9] with the Perdew-Burke-Ernzerhof (PBE)[10] exchange correlation functional. The projected augmented wave (PAW)[10] potentials have been used. A Γ-centered 5×5×5 Monkhorst-Pack grid for the Brillouin zone sampling[12] and a cutoff energy of 600 eV for the plane wave expansion were found to get convergent lattice parameters. Both the cell and atomic relaxations were carried out until the residual forces are below 0.02 eV/Å. A Monkhorst-Pack *k*-point mesh of 7×7×7 was used for the calculation of the linear and nonlinear optical properties.

The imaginary part of the dielectric function due to direct inter-band transitions is given by the expression:

$$\varepsilon_2(\mathrm{h}\omega) = \frac{2e^2\pi}{\Omega\varepsilon_0}\sum_{k,v,c}\left|\left\langle\psi_k^c\left|u\cdot r\right|\psi_k^v\right\rangle\right|^2\delta(E_k^c - E_k^v - E) \quad \ldots\ldots\ldots\ldots (1)$$

where Ω, ω, u, v and c are the unit-cell volume, photon frequencies, the vector defining the polarization of the incident electric field, valence and conduction bands, respectively. The real part of the dielectric function is obtained from ε_2 by a Kramers-Kronig transformation:

$$\varepsilon_1(\omega) = 1 + (\frac{2}{\pi})\int_0^{+\infty} d\omega' \frac{\omega'^2\varepsilon_2(\omega)}{\omega'^2 - \omega^2} \quad \ldots\ldots\ldots\ldots (2)$$

The refractive index $n(\omega)$ can be obtained based on ε_1 and ε_2.

In calculation of the static $\chi^{(2)}$ coefficients, the so-called length-gauge formalism derived by Aversa and Sipe[13] and modified by Rashkeev et al[14] is adopted, which has proven to be successful in calculating the second order susceptibility for semiconductors and insulators. In the static case, the imaginary part of the static second-order optical susceptibility can be expressed as:

$$\chi^{abc} = \frac{e^3}{\mathrm{h}^2\Omega}\sum_{nml,k}\frac{r_{nm}^a(r_{ml}^b r_{ln}^c + r_{ml}^c r_{ln}^b)}{2\omega_{nm}\omega_{ml}\omega_{ln}}[\omega_n f_{ml} + \omega_m f_{ln} + \omega_l f_{nm}]$$
$$+\frac{ie^3}{4\mathrm{h}^2\Omega}\sum_{nm,k}\frac{f_{nm}}{\omega_{mn}^2}[r_{nm}^a(r_{mn;c}^b + r_{mn;b}^c) + r_{nm}^b(r_{mn;c}^a + r_{mn;a}^c) + r_{nm}^c(r_{mn;b}^a + r_{mn;a}^b)]$$

……(3)

where r is the position operator, $\hbar\omega_{nm} = \hbar\omega_n - \hbar\omega_m$ is the energy difference for the bands m and n, $f_{mn} = f_m - f_n$ is the difference of the Fermi distribution functions, subscripts a, b, and c are Cartesian indices, and $r^b_{mn;a}$ is the so-called generalized

derivative of the coordinate operator in *k* space,

$$r^{b}_{nm;a} = \frac{r^{a}_{nm}\Delta^{b}_{mn} + r^{b}_{nm}\Delta^{a}_{mn}}{\omega_{nm}} + \frac{i}{\omega_{nm}} \times \sum_{l} (\omega_{lm} r^{a}_{nl} r^{b}_{lm} - \omega_{nl} r^{b}_{nl} r^{a}_{lm}) \quad \ldots\ldots\ldots\ldots (4)$$

where $\Delta^{a}_{nm} = (p^{a}_{nn} - p^{a}_{mm}) / m$ is the difference between the electronic velocities at the bands *n* and *m*.

As the nonlinear optical coefficients is sensitive to the momentum matrix, much finer k-point grid and large amount of empty bands are required to obtain a convergent $\chi^{(2)}$ coefficient. The $\chi^{(2)}$ coefficients here were calculated from PBE wave functions and a scissor operator has been added to correct the conduction band energy (corrected to the experimental gap), which has proven to be reliable in predicting the second order susceptibility for semiconductors and insulators.

3. Figures and Tables

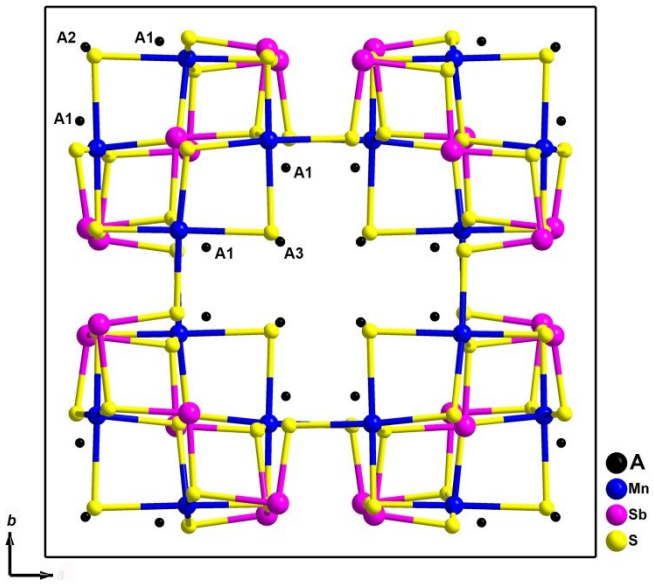

Figure S1. The unit cell of $A_3Mn_2Sb_3S_8$ with three crystallographically unique A atoms outlined.

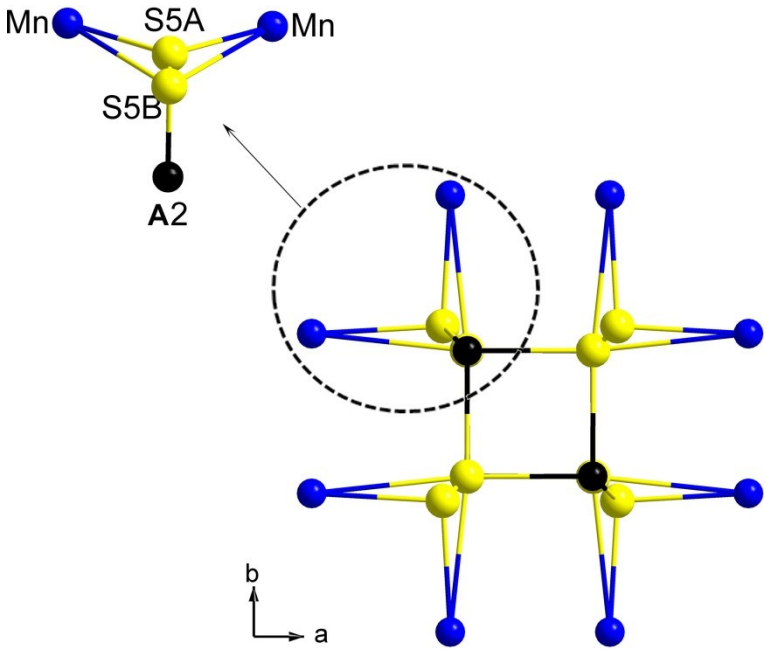

Figure S2. The local coordination environment of the split atom S5 in the structure of $A_3Mn_2Sb_3S_8$.

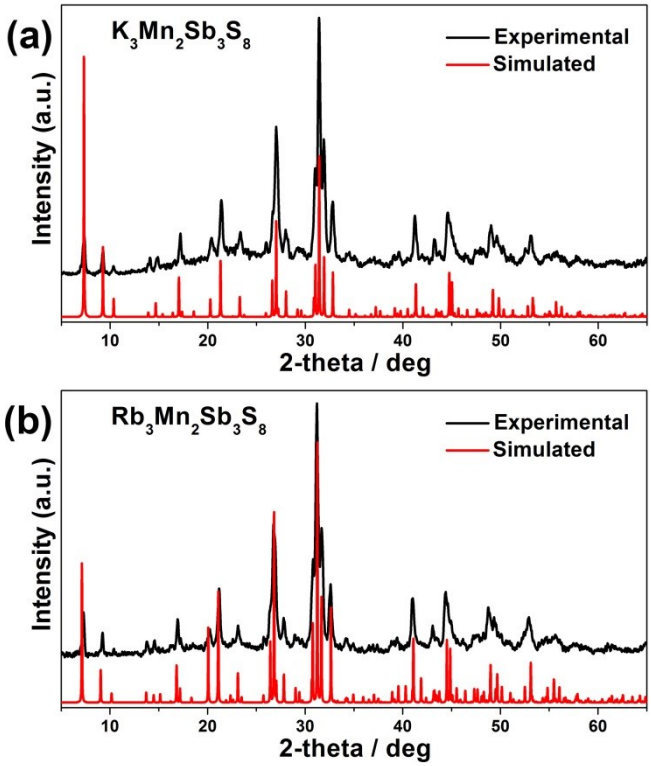

Figure S3. The experimental (black) and simulated (red) powder XRD of (a) $K_3Mn_2Sb_3S_8$ and $Rb_3Mn_2Sb_3S_8$.

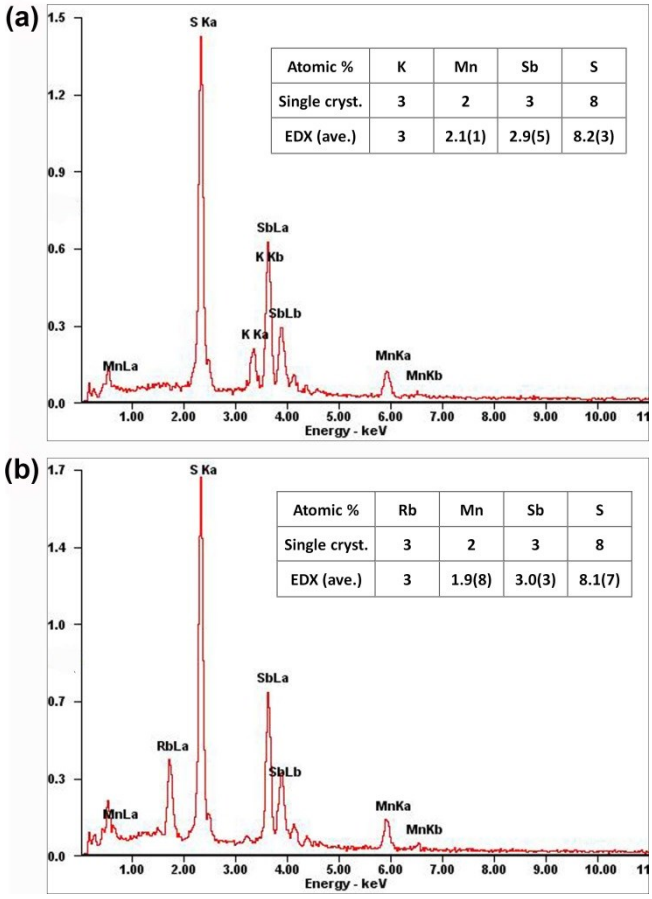

Figure S4. EDX results and the obtained compositions of (a) $K_3Mn_2Sb_3S_8$ and (b)$Rb_3Mn_2Sb_3S_8$.

Table S1. Atomic coordinates and equivalent isotropic displacement parameters of $A_3Mn_2Sb_3S_8$ (A = K and Rb).

Atom	*Wyckoff*	*x*	*y*	*z*	$U_{(eq)}$*	*Occu.*
			$K_3Mn_2Sb_3S_8$			
K1	16*j*	0.0628(2)	0.2076(2)	0.0826(2)	0.150(6)	1.0
K2	8*i*	0.0739(3)	0.0739(3)	0.4087(5)	0.014(2)	0.911(4)
K3	8*i*	0.072(2)	0.072(2)	0.264(4)	0.007(2)	0.089(4)
Mn	16*j*	0.2426(2)	0.4059(2)	0.0947(3)	0.0218(7)	1.0
Sb1	8*i*	0.2383(2)	0.2383(2)	0.3398(2)	0.0312(6)	1.0
Sb2	16*j*	0.0773(2)	0.4024(2)	0.3663(2)	0.0371(6)	1.0
S1	8*i*	0.2580(4)	0.2580(4)	0.0512(7)	0.038(2)	1.0
S2	16*j*	0.2305(4)	0.3847(3)	0.3197(5)	0.032(2)	1.0
S3	16*j*	0.0569(3)	0.2608(3)	0.3660(5)	0.031(2)	1.0
S4	16*j*	0.0917(4)	0.4037(4)	0.0747(4)	0.032(2)	1.0
S5A	8*i*	0.3971(9)	0.3971(9)	0.1056(2)	0.043(4)	0.5
S5B	8*i*	0.0744(2)	0.0744(2)	0.572(2)	0.060(6)	0.5
			$Rb_3Mn_2Sb_3S_8$			
Rb1	16*j*	0.0610(5)	0.2011(5)	0.0806(8)	0.112(2)	1.0
Rb2	8*i*	0.0735(3)	0.0735(3)	0.4076(7)	0.0314(2)	0.665(4)
Rb3	8*i*	0.0685(9)	0.0685(9)	0.262(2)	0.065(5)	0.335(4)
Mn	16*j*	0.2424(2)	0.4061(2)	0.0935(4)	0.0123(9)	1.0
Sb1	8*i*	0.2371(2)	0.2371(2)	0.3373(3)	0.0231(7)	1.0
Sb2	16*j*	0.0776(2)	0.4026(2)	0.3654(2)	0.029(7)	1.0
S1	8*i*	0.2582(5)	0.2582(5)	0.0496(9)	0.024(2)	1.0
S2	16*j*	0.2296(5)	0.3826(4)	0.3165(7)	0.023(2)	1.0
S3	16*j*	0.0562(4)	0.2603(4)	0.3666(7)	0.024(2)	1.0
S4	16*j*	0.0907(4)	0.4031(4)	0.0740(6)	0.022(2)	1.0
S5A	8*i*	0.3947(2)	0.3947(2)	0.101(2)	0.029(5)	0.5
S5B	8*i*	0.0754(2)	0.0754(2)	0.578(3)	0.038(6)	0.5

*$U_{(eq)}$ is defined as one-third of the trace of the orthogonalized U_{ij} tensor.

Table S2. Selected bond lengths (Å) and angles (°) of $A_3Mn_2Sb_3S_8$ (A = K and Rb).

	$K_3Mn_2Sb_3S_8$	**$Rb_3Mn_2Sb_3S_8$**
Mn−S4	2.587(7)	2.598(8)
Mn−S1	2.587(7)	2.587(8)
Mn−S3	2.616(6)	2.602(8)
Mn−S2	2.624(6)	2.614(8)
Mn−S5	2.644(2)	2.606(2)
Mn−S3	2.711(6)	2.696(9)
Sb1−S1	2.437(8)	2.452(2)
Sb1−S2	2.513(6)	2.497(7)
Sb1−S2	2.513(6)	2.497(7)
Sb2−S4	2.425(5)	2.432(7)
Sb2−S3	2.441(6)	2.454(7)
Sb2−S2	2.687(7)	2.675(8)
∠S4–Mn–S1	94.0(3)	93.9(3)
∠S4–Mn–S3	90.4(2)	91.0(2)
∠S1–Mn–S3	175.3(3)	174.9(3)
∠S4–Mn–S2	90.4(2)	89.9(3)
∠S1–Mn–S2	93.7(2)	93.0(3)
∠S3–Mn–S2	87.9(2)	88.6(3)
∠S4–Mn–S5	175.2(4)	173.8(5)
∠S1–Mn–S5	81.5(4)	80.2(5)
∠S3–Mn–S5	94.1(4)	94.9(4)
∠S2–Mn–S5	91.4(5)	92.3(6)
∠S4–Mn–S3	84.0(2)	84.5(2)
∠S1–Mn–S3	92.4(2)	92.5(3)
∠S3–Mn–S3	86.4(2)	86.4(3)
∠S2–Mn–S3	172.0(2)	172.4(2)
∠S5–Mn–S3	94.6(5)	93.8(6)
∠S1–Sb1–S2	93.9(2)	93.7(3)
∠S1–Sb1–S2	93.9(2)	93.7(3)
∠S2–Sb1–S2	95.6(3)	95.3(4)
∠S4–Sb2–S3	93.6(2)	93.5(3)
∠S4–Sb2–S3	94.1(2)	94.8(2)
∠S3–Sb2–S2	91.6(2)	91.1(2)

4. References

1. P. Kubelka, An article on optics of paint layers, *Z. Tech. Phys.*, 1931, **12**, 593–601.

2. S. K. Kurtz and T. T. Perry, A powder technique for the evaluation of nonlinear optical materials, *J. Appl. Phys.*, 1968, **39**, 3798–3813.

3. M. J. Zhang, X. M. Jiang, L. J. Zhou and G. C. Guo, Two phases of Ga_2S_3: promising infrared second-order nonlinear optical materials with very high laser induced damage thresholds, *J. Mater. Chem. C*, 2013, **1**, 4754–4760.

4. *CrystalClear* Version 1.3.5; Rigaku Corp.: Woodlands, TX, 1999.

5. G. M. Sheldrick, A short history of SHELX, *Acta Crystallogr., Sect. A: Found. Crystallogr.* 2008, 112–122.

6. L. M. Gelato and E. *J.* Parthe, STRUCTURE TIDY–a computer program to standardize crystal structure data, *Appl. Crystallogr.* 1987, **20**, 139–143.

7. G. Kresse, VASP, 5.3.5; http://cms.mpi.univie.ac.at/vasp/vasp/vasp.html.

8. G. Kresse, J. Furthmuller, Efficient iterative schemes for ab initio total-energy calculations using a plane-wave basis set, *Phys. Rev. B: Condens. Matter*, 1996, 11169–11186.

9. G. Kresse and D. Joubert, From ultrasoft pseudopotentials to the projector augmented-wave method, *Phys. Rev. B: Condens. Matter*, 1999, **59**, 1758–1775.

10. P. E. Blochl, Projector augmented-wave method, *Phys. Rev. B: Condens. Matter*, 1994, **50**, 17953–17979.

11. J. P. Perdew, K. Burke and M. Ernzerhof, Generalized gradient approximation made simple, *Phys. Rev. Lett.*, 1996, **77**, 3865–3868.

12. D. J. Chadi, Special points for Brillouin-zone integrations, *Phys. Rev. B: Condens. Matter*, 1976, **16**, 1746–1747.

13. C. Aversa and J. E. Nonlinear optical susceptibilities of semiconductors: Results with a length-gauge analysis, Sipe, *Phys. Rev. B*, 1995, **52**, 14636–14645.

14. S. N. Rashkeev, W. R. L. Lambrecht and B. Segall, Efficient ab initio method for the calculation of frequency-dependent second-order optical response in semiconductors, *Phys. Rev. B*, 1998, **57**, 3905–3919.